



Full Length Article

Development of Ca/KIT-6 adsorbents for high temperature CO₂ capture

Hongman Sun^a, Christopher M.A. Parlett^{b,*}, Mark A. Isaacs^c, Xiaotong Liu^a, George Adwek^d, Jianqiao Wang^d, Boxiong Shen^{d,*}, Jun Huang^{e,*}, Chunfei Wu^{a,f,g,*}

^a School of Engineering and Computer Science, University of Hull, Hull HU6 7RX, UK

^b European Bioenergy Research Institute, University of Aston, Birmingham B4 7ET, UK

^c Department of Chemistry, University College London, London WC1H 0AJ, UK

^d School of Energy & Environmental Engineering, Hebei University of Technology, Tianjin 300401, China

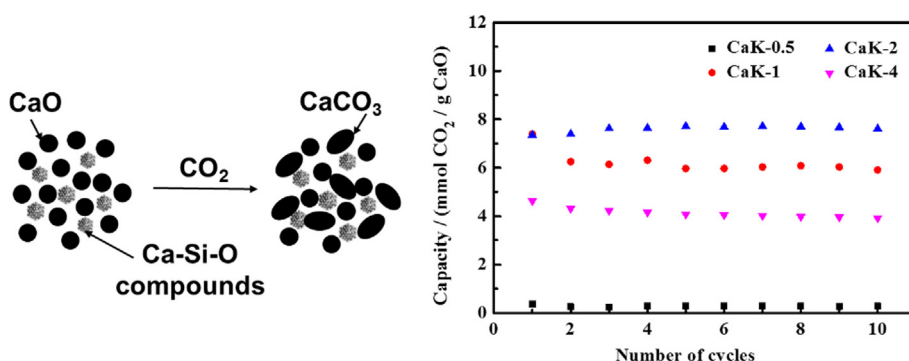
^e School of Chemical and Biomolecular Engineering, The University of Sydney, Sydney, NSW 2037, Australia

^f Key Laboratory of Ocean Energy Utilization and Energy Conservation of Ministry of Education, Dalian University of Technology, Dalian 116024, China

^g School of Chemistry and Chemical Engineering, Queen's University Belfast, Belfast BT7 1NN, UK



GRAPHICAL ABSTRACT



ARTICLE INFO

Keywords:

CaO
Mesoporous silica
KIT-6
CO₂ capture
Adsorbent

ABSTRACT

The incorporation of CaO into an inert porous solid support has been identified as an effective approach to improve the stability of adsorbents for CO₂ capture. In this work, we focus on enhancing the capacity of carbon capture and cyclic stability of CaO by impregnating CaO particles into a three-dimensional mesoporous silica (KIT-6) support. At a low CaO loading, the three-dimensional mesoporous support was filled with CaO nanoparticles. The further increase of CaO loading resulted in the aggregation of CaO particles on the external surface of the support material, as identified by electron microscopy analysis. These CaO/KIT-6 adsorbents show excellent high-temperature CO₂ carbonation/calcination stability over multiple cycles of CaO carbonation and calcination. The enhancement of the performance of carbon capture is attributed to the interaction between CaO and the silica skeleton of KIT-6 through the formation of interfacial CaSiO₃ and Ca₂SiO₄ which enhanced the resistance of CaO sintering.

* Corresponding authors at: School of Engineering and Computer Science, University of Hull, Hull HU6 7RX, UK (C. Wu).

E-mail addresses: parlett1@aston.ac.uk (C.M.A. Parlett), shenbx@hebut.edu.cn (B. Shen), jun.huang@sydney.edu.au (J. Huang), c.wu@qub.ac.uk (C. Wu).

<https://doi.org/10.1016/j.fuel.2018.07.044>

Received 16 March 2018; Received in revised form 6 July 2018; Accepted 9 July 2018

0016-2361/ © 2018 Published by Elsevier Ltd.

1. Introduction

CO₂ emissions are major contributions to climate change and ocean acidification [1,2]. Natural concentration of atmospheric CO₂ ranges from 180 to 300 ppm [3]. However, the current concentration of CO₂ is over 407 ppm owing to the combustion of fossil fuels [4,5]. With global economic growth, especially for developing countries, the atmospheric CO₂ concentration is likely to be further increased. Thus technologies for carbon capture are gaining worldwide interest [6–8]. At high temperature (~700 °C), CaO-based adsorbent can be used for carbon capture and for sorption-enhanced hydrogen reaction [9]. In addition, the production of synthetic natural gas could be directly produced from the captured CO₂ using multifunctional catalytic adsorbents [10].

Calcium oxide is a promising high-temperature CO₂ adsorbent, due to its high theoretical capacity of carbon capture (17.8 mmol CO₂ g⁻¹ CaO), and its low cost and high abundance [11–13]. The major limitation of CaO-based adsorbents, in particular at high temperature, is their intrinsic low resistance to particle sintering during the multicycle operation [14–16]. Thus a poor carbonation/calcination reversibility is obtained due to the inhibition of CO₂ diffusion through CaCO₃, a product formed on the surface of CaO during carbon capture. Several methods have been reported to enhance the capacity of CO₂ uptake and to reduce the sintering of CaO particles for carbon capture using CaO-based adsorbents. One of these methods is called controlled precipitation which can produce small and uniform porous CaO particles [17]. Furthermore, the pre-treatment of adsorbents through steam hydration [18,19] and acid modification [20] has been investigated to introduce cracks within the CaO particles to reduce the blockage of pores during carbon capture [19]. Manovic et al. [15] investigated steam reactivation of a spent adsorbent. It was reported that both the reversibility and the capacity of CO₂ capture were enhanced for the reactivated adsorbent compared to the parent material. In addition, the pre-treatment of limestone using acetic acid, conducted by Li et al [20], significantly decreased the crystallite size of CaO, enhancing the resistance to CaO sintering.

The addition of a second metal oxide represents another alternative strategy to improve the sintering resistance of CaO-based adsorbents [21,22]. Metal oxides such as MgO [21], Y₂O₃ [23] and CeO₂ [24] can act as a discrete second phase or react with CaO producing a mixed oxide material such as Ca₁₂Al₁₄O₃₃ [22], CaTiO₃ [25], CaZrO₃ [26] and CaSiO₃ [27]. Albrecht et al. introduced 20 wt% MgO into a CaO-based adsorbent, which enhanced the stability of the adsorbent owing to the finely dispersed MgO species [21]. Zhang et al. [23] synthesized a series of Y₂O₃-modified CaO adsorbents via a sol-gel method. With the introduction of Y₂O₃, the carbonation of CaO was significantly improved. In addition, a mixed oxide (Ca₁₂Al₁₄O₃₃) was produced via the addition of Al(NO₃)₃·9H₂O. The authors reported a high CO₂ capture capacity of 10.2 mmol g⁻¹ over 13 cycles carbonation and calcination using the Ca₁₂Al₁₄O₃₃ enhanced adsorbent [22]. However, the addition of expensive oxides, e.g. Y₂O₃, CeO₂ and TiO₂, will reduce the economic viability of the carbon capture process.

SiO₂ represents a cost-effective and widely available sinter-resistant metalloid oxide. Zhao et al. described a sol-gel method to synthesize a porous SiO₂ supported CaO, with an optimal Si:Ca ratio possessing a capture capacity of 7.5 mmol g⁻¹ [27]. The material displayed an excellent stability over 50 cycles of carbonation and calcination due to the presence of Ca-O-Si and specific porosity of the adsorbent. Mesoporous silicas, MCM-48 modified with organosilane amines [28] and CaO/SBA-15 [29], have shown high capacities of CO₂ capture, revealing the feasibility of using both three-dimensional Ia3d and two-dimensional P6mm architectures as the support materials for CaO particles. KIT-6, a mesoporous SiO₂ combining the Ia3d architecture akin to MCM-48 but with larger pore diameters, has attracted attention in recent years due to its optimal physicochemical properties that enhance metal dispersion and subsequent accessibility of reactants [30,31].

Here we applied KIT-6, a highly stable CO₂ inert silica framework,

as a support for CaO which was employed for high-temperature CO₂ carbonation. To our knowledge, this is the first time to use the mesoporous silica KIT-6 in CaO based CO₂ capture system. Its physicochemical properties could enhance the stability of CaO, potentially via the formation of interfacial Ca-rich mixed oxide phases, whilst simultaneously allowing superior carbonation/calcination reversibility due to the reduced effect of pore blockage arising from its three-dimensional pore structure. The effect of CaO doping concentration and the resulting influence on CO₂ capture were studied within a fixed bed reactor, with characterisations by in-situ X-ray diffraction (XRD), nitrogen adsorption-desorption, scanning electron microscopy (SEM) coupled to an energy dispersive X-ray spectroscopy (EDX) and transmission electron microscopy (TEM).

2. Experimental sections

2.1. Materials preparation

Calcium nitrate tetrahydrate (Ca(NO₃)₂·4H₂O, 99.0% purity, Sigma-Aldrich) was used as the CaO precursor, with the KIT-6 mesoporous silica support synthesized by a non-ionic surfactant templating approach according to the procedure reported by Kleitz et al. [32].

The KIT-6 supported CaO-based adsorbents were synthesized using wet impregnation method. In a typical experiment, 4.217 g Ca(NO₃)₂·4H₂O, corresponding to 1 g CaO, was dissolved in 25 mL distilled water. After the precursor was completely dissolved under continuous stirring at 80 °C, 0.5 g KIT-6 was then added to the calcium nitrate solution. The solution was kept static for 24 h at room temperature, prior to the evaporation of water at 80 °C. The solid product was calcined in a muffle furnace at 500 °C for 6 h with a heating rate of 2 °C min⁻¹. The resulting adsorbents are denoted as CaK-x, where x represents the weight ratio of CaO to KIT-6, which was varied to give values of 0.5, 1, 2 and 4. A commercial CaO (Sigma-Aldrich, 99.99%), dried overnight at 130 °C, was used as a reference adsorbent.

2.2. Cyclic CO₂ capture tests

The performance of the CaK-x adsorbents for carbon capture was measured using an SDT Q600 thermogravimetric analyzer (TGA). The adsorbent (~10 mg) was loaded in an alumina crucible and activated by heating to 850 °C at a ramp rate of 15 °C min⁻¹ under pure N₂ flow (1 bar, 100 mL min⁻¹) with the sample held at temperature for 10 min. The carbonation was performed under 15% CO₂ in N₂ (1 bar, 100 mL min⁻¹) at 600 °C for 30 min. The atmosphere was then switched to pure N₂ (1 bar, 100 mL min⁻¹) and the sample was heated to 800 °C at 15 °C min⁻¹ and held for 10 min. The cycles of CaO carbonation/calcination were repeated 10 times.

In order to compare the performance of CO₂ capture using the CaK-x adsorbents, the capacity of CO₂ capture and the carbonation conversion are used.

The capacity of CO₂ capture was calculated according to the following formula:

$$\text{Uptake capacity (mmol g}^{-1}\text{)} = \text{mmol of CO}_2\text{/g of CaO} \quad (1)$$

The carbonation conversion of the sample was calculated using Eq. (2).

$$X_N (\%) = \frac{m_N - m_1}{m_0 - m_1} \cdot \frac{M_{\text{CaO}}}{M_{\text{CO}_2}} \cdot 100\% \quad (2)$$

where X_N is carbonation conversion of sample, N is the number of cycles, m_0 is the initial mass of sample, b is the content of CaO in the synthesized sample, m_N is mass of the carbonated sample after N cycles, m_1 is mass of sample after calcination (mass of sample after each calcination is the same), and M_{CaO} and M_{CO_2} are mole mass of CaO and CO₂, respectively.

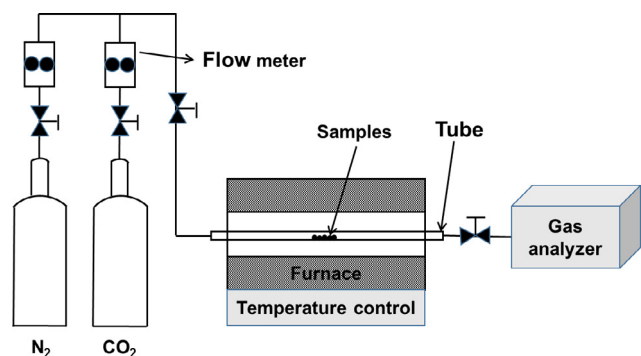


Fig. 1. Schematic diagram of the atmospheric carbonation/calcination reactor system.

2.3. Fixed bed CO₂ capture performance

A fixed-bed reactor coupled to a gas analyser (as shown in Fig. 1) was used to determine CO₂ capture performance of the CaK-x adsorbents in a temperature swing process. 200 mg of powdered CaO-based adsorbent was loaded into a tube reactor. The sample was retained in place with quartz wool plugs, and activated by calcination at 800 °C in 100% N₂ (1 bar, 100 mL min⁻¹) for 30 min prior to the temperature swing process evaluation. When the temperature was decreased to 350 °C, the carbonation of CaO was carried out in a 15% CO₂/N₂ mixture (1 bar, 100 mL min⁻¹) with a heating rate of 10 °C min⁻¹. It was followed by a calcination of CO₂ in 100% N₂ (1 bar, 100 mL min⁻¹) when the temperature was increased to 900 °C. The temperature swing process was repeated a minimum of 3 times to evaluate and ensure the reproducibility of experimental results.

2.4. Characterization of adsorbent

In-situ XRD was conducted to elucidate the crystalline phase composition of the CaK-x adsorbents after thermal activation. XRD patterns were collected using an Anton-Paar XRK-900 high-pressure XRD cell fitted to a Bruker d8 advance XRD, which was equipped with a Cu ka X-ray source (1.54 Angstroms) and a 192-channel Lynxeye high-speed strip detector. Sample activation was carried out at 850 °C under flowing nitrogen (1 bar, 50 mL/min) for 1 h, using a heating rate of 10 °C min⁻¹ before cooling to 50 °C for data collection. Scans were collected from 10° to 80° 2θ with a step size of 0.1° and dwell time of 1 s. Rietveld refinement for phase quantification was performed using DIFFRAC.EVA software and crystallite size were determined through application of the Scherrer equation to the peaks at 37.45° (CaO), 26.85° (CaSiO₃) and 34.32° (Ca₂SiO₄).

Nitrogen adsorption-desorption isotherms were measured using ASAP 2000 analyzer at 77 K. Barrett-Emmett-Teller (BET) surface area was measured using the adsorption branch data in the relative pressure (P/P₀) range from 0.06 to 0.2 [33]. Scanning electron microscopy (SEM) and transmission electron microscopy (TEM) were conducted on a Stereoscan 360 SEM coupled to an energy dispersive X-ray spectrometer (EDX) and a JEOL 2010 TEM, respectively. For SEM imaging, samples were gold sputter coated to reduce charging whilst for TEM analysis samples were ground, dispersed in acetone, and drop-cast on carbon coated Cu grids.

3. Results and discussion

3.1. Adsorbent characterization

The nature of the Ca phases present in the adsorbents, after high-temperature activation, was evaluated by in-situ XRD, with the corresponding patterns of CaK-x reported in Fig. 2. A broad peak centred

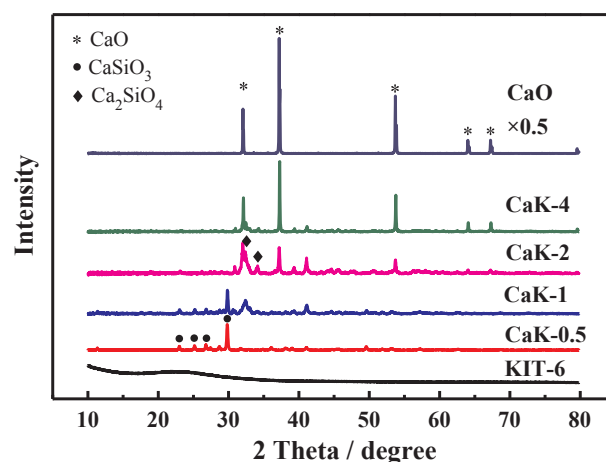


Fig. 2. In-situ XRD analysis of CaO-based adsorbents.

around 23° is observed in KIT-6, corresponding to the amorphous silica of the support framework. At the lower CaO loadings, the CaK-0.5 and the CaK-1 exhibit weak features at 23.15°, 25.3°, 26.85° and 30.02° arising from crystalline CaSiO₃, which originates at the interface of CaO and KIT-6. Increasing CaO loading, from the CaK-1 to the CaK-4, results in a transition to a more calcium-rich silicate, Ca₂SiO₄, indexed from features at 32.57° and 34.32°. The subsequent formation of CaO with diffraction peaks at 32.00°, 37.45°, 54.00°, 64.33°, and 67.56° is observed. A quantitative analysis of the phase compositions and average crystallite sizes of the Ca species present in the four adsorbents, and a reference bulk CaO, are reported in Table 1. In addition to the shift to a more Ca-rich silicate with increasing CaO loading, there is a concurrent decrease in the average size of the CaSiO₃ phase and an increase in the Ca₂SiO₄ phase, albeit with both showing a similar upper limit (~40 nm). It potentially indicates an upper limit on the degree of diffusion between these two oxides. The average crystallite size of CaO phase is increased with the increase of CaO loading, reaching a maximum of 87 nm, which is still significantly smaller than the commercial bulk CaO material. We propose an adsorbent structure of CaO nanoparticles supported on calcium silicate, either CaSiO₃ and Ca₂SiO₄, which are interfacial species between the CaO and the SiO₂ KIT-6 framework. The significant presence, in both quantity and size, of calcium silicates suggests a reasonable degree of diffusion between the two solids.

N₂ adsorption-desorption isotherms and pore-size distributions are utilised to investigate the porous structure of the parent KIT-6 silica and the CaO doped adsorbents, as shown in Fig. 3. Textural properties derived from different CaO-based adsorbents are summarized in Table 2. The parent KIT-6 support displays the characteristic type IV isotherm of a mesoporous solid, with average mesopore diameter of 5.5 nm. The isotherms of the CaK-x samples exhibit either type II isotherms or type IV with hysteresis shift to higher relative pressure. This reflects a loss in the mesoporous of the silica framework, through the filling/capping with calcium silicate/CaO crystallites, which is reflected in the materials surface areas, pore volumes and BJH pore size distributions. As for the CaK-0.5 and CaK-1, both two adsorbents exhibit a pore size distribution ranging from 2 nm to 10 nm, which is not observed in a CaO

Table 1
Phase composition and average crystallite size of CaO-based adsorbents.

Sample	CaO	Ave. Size	CaSiO ₃	Ave. Size	Ca ₂ SiO ₄	Ave. Size
CaK-0.5	0%	n.a.	100%	45 nm	0%	n.a.
CaK-1	4%	40 nm	66%	35 nm	30%	18 nm
CaK-2	15%	40 nm	0%	n.a.	85%	30 nm
CaK-4	54%	87 nm	0%	n.a.	46%	37 nm
CaO	100%	120 nm	0%	n.a.	0%	n.a.

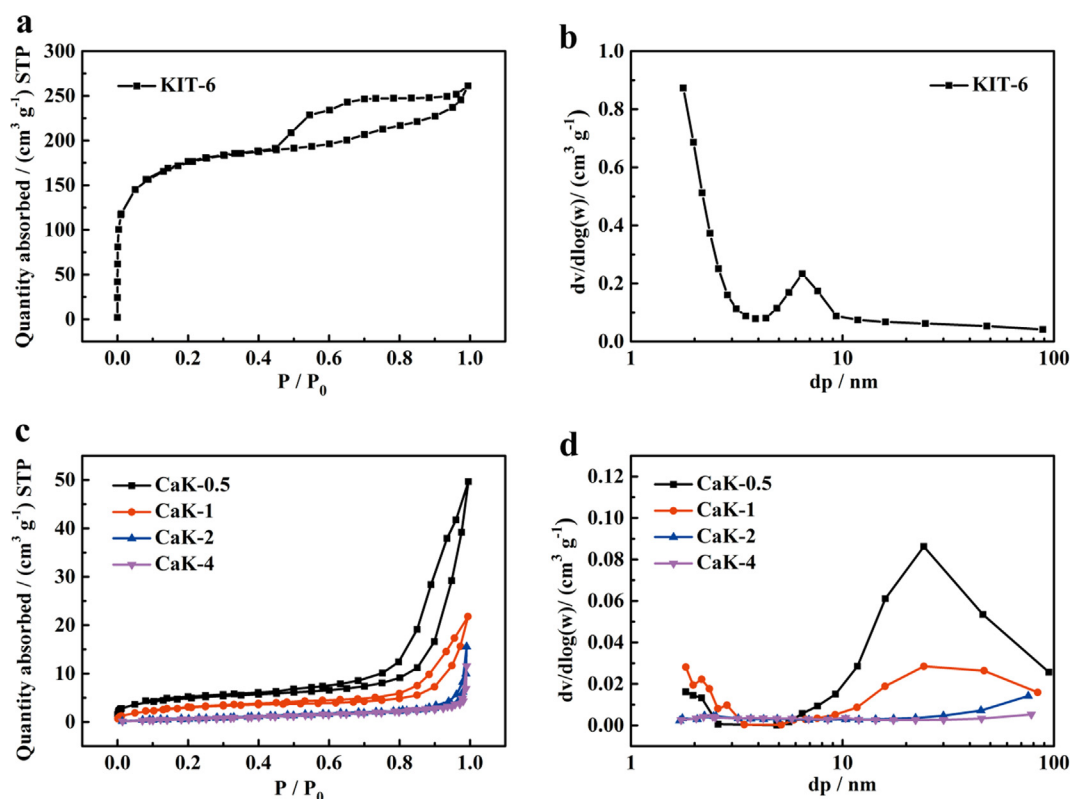


Fig. 3. N_2 adsorption-desorption isotherms (a: KIT-6; c: CaO-based adsorbents) and pore size distribution calculated from the BJH adsorption branch (b: KIT-6; d: CaO-based adsorbents).

Table 2
Textural properties derived from different CaO-based adsorbents.

Samples	$S_{BET}/(m^2/g)$	$S_{micro}/(m^2/g)$	$S_{meso}/(m^2/g)$	$V_{total}/(cm^3/g)$	$V_{micro}/(cm^3/g)$	$V_{meso}/(cm^3/g)$
KIT-6	545	265	280	0.40	0.11	0.29
CaK-0.5	16.2	8.6	7.8	0.08	0.005	0.075
CaK-1	11.1	7.0	4.1	0.04	0.003	0.035
CaK-2	2.9	1.0	1.9	0.007	0.003	0.004
CaK-4	2.7	1.0	1.7	0.005	0.002	0.003

sample derived from limestone [23,34]. This is attributed to the three-dimensional mesoporous structure of the KIT-6 support. In addition, similar surface area ($\sim 12 m^2/g$) and pore volume ($\sim 0.05 cm^3/g$) of CaO-based sorbents are reported in literature [14,23]. The hysteresis of the CaK-2 and CaK-4 samples is observed at higher pressure, which reflects larger dimensions caused by the interparticle voids between the Ca phases.

SEM micrographs of the parent KIT-6 and the CaK-x adsorbents are presented in Fig. 4. The morphology and surface topography of the KIT-6 comprises angular particulates with a relatively flat surface. The incorporation of CaO in the silica KIT-6 support results in a significant surface transformation to a rougher surface which is proportional to the loading of CaO. For the CaK-0.5, this effect is minimal with only a slight degree of surface roughening, which is attributed to the formation of only the mixed oxide phase, as identified by XRD. With the increase of CaO loading, the external surface is transformed into a sponge-like coating, which agrees with the proposed model from the XRD results, i.e. the deposition of CaO upon the interfacial calcium silicate. When the CaO loading was further increased (CaK-2), the parent silica particle morphology is not visible, being completely covered with CaO particles. Elemental analysis (EDX), representative spectra shown in Fig. 4, confirms the successful synthesis of step-wise increase of CaO content, with loadings of 27.1, 39.4, 57.1 and 64.1 wt% for the CaK-0.5, CaK-1, CaK-2

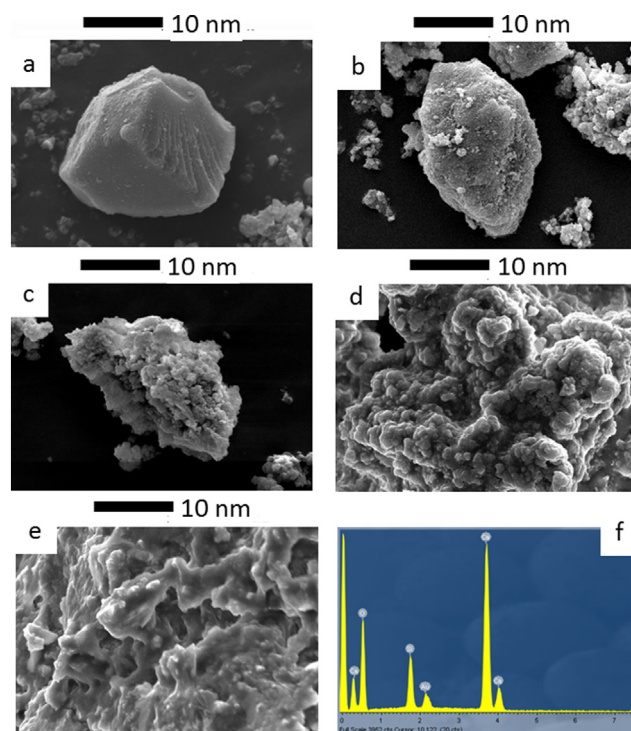


Fig. 4. SEM images of (a) parent KIT-6, (b) CaK-0.5, (c) CaK-1, (d) CaK-2 and (e) CaK-4, with (f) representative EDX spectra for CaK-2.

and CaK-4, respectively.

TEM was employed to observe the internal mesopore structure, as shown in Fig. 5. For the parent KIT-6, ordered mesoporosity is clear, in agreement with nitrogen porosimetry. With the increase of CaO doping,

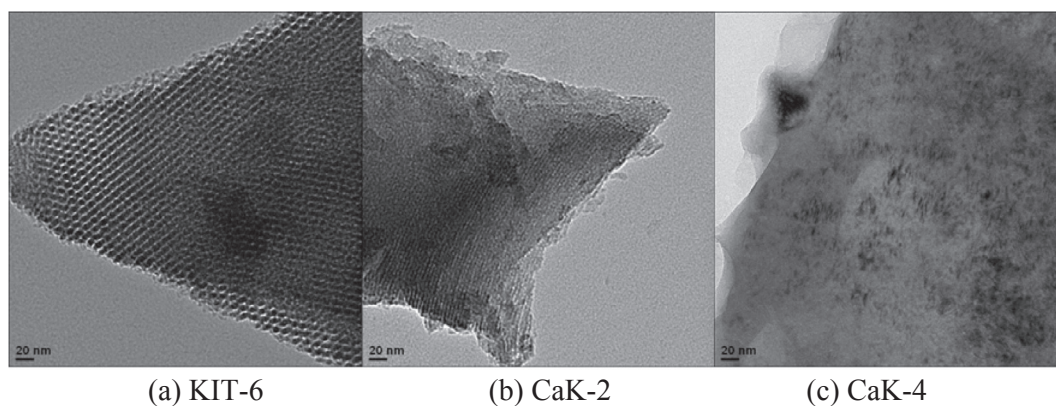


Fig. 5. TEM images of parent KIT-6 and CaK-x adsorbents.

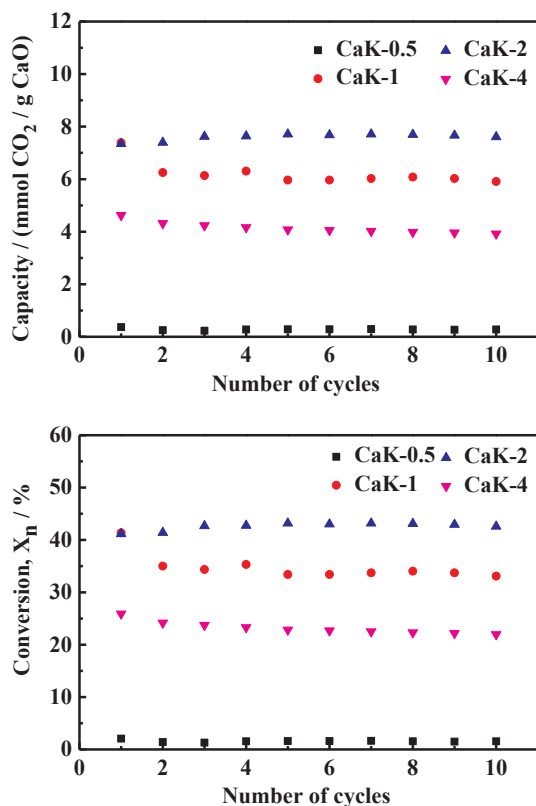


Fig. 6. Cyclic capture capacity and conversion of different adsorbents per gram of CaO at 650 °C.

the mesostructure becomes less apparent. The CaK-2 only shows a small degree of pore periodicity. Combined with the nitrogen porosimetry data for the CaK-2, the pores of the parent KIT-6 are suggested to be blocked, which can be attributed to the growth of external crystallites, as observed by SEM (Fig. 4). At the highest Ca loading, no mesopore structure is apparent indicating complete pore filling which agrees with the nitrogen porosimetry results.

3.2. CO₂ carbonation and calcination

Fig. 6 shows the capacity of CO₂ capture and the conversion of the four CaO-based adsorbents for 10 cycles of carbonation and calcination. At the lowest CaO loading, the CaK-0.5 exhibits negligible capacity of carbon capture, reflecting the inability of the calcium silicate to capture CO₂. The CaK-1 shows a good initial CO₂ capture during the first cycle of carbonation/calcination, but the capacity of carbon capture is

decreased after 10 cycles. This is also apparent for the CaK-4, with an initial capacity of 4.6 mmol g⁻¹ decreasing to 3.9 mmol g⁻¹ after 10 cycles of carbonation/calcination, reflecting a 15% decrease in carbon capture capacity. In contrast, the CaK-2 is stable during the cycles of carbonation/calcination, and exhibits the highest capacity of CO₂ capture. This is attributed to the optimum synergy between the active CaO and the interface within this material, which may inhibit further sintering of CaO-based adsorbents [35]. Compared to the theoretical maximum CO₂ capacity of CaO, this optimum material exhibits a conversion of CaO to CaCO₃ of ~40%, indicating that full CaO utilization is not achieved even at the relatively small nanoparticle sizes of 40 nm.

The temperature swing process was employed to evaluate the influence of carbonation (CO₂ capture) and calcination (CO₂ release) temperature on carbon capture for the two optimal materials, the CaK-2 and CaK-4, with the results presented in Fig. 7. For both materials, the carbonation occurs at 400 °C and 600 °C, and the calcination happens at 700 °C and 850 °C, respectively. It is suggested that the carbonation activation energies of surface and bulk transformations are 88.9 ± 3.7 and 179.2 ± 7.02 kJ mol⁻¹ for temperatures below and above 515 °C, respectively [36,37]. The increase in activation energy, with temperature, is attributed to the inhibition of CO₂ diffusion through the initially formed surface CaCO₃. The capture profiles in both CaK-2 and CaK-4 are identical, indicating the formation of CaCO₃ layer prior to bulk carbonation at 600 °C for both CaK-2 and CaK-4. In contrast, the release profiles are different because the CaK-2 releases proportionally more CO₂ at the lower temperature (700 °C), which reflects the small CaO crystallite present in the CaK-2. This more facile regeneration may also contribute to the greater stability of the CaK-2 during the carbonation/calcination cycle testing compared to the CaK-4 in Fig. 6.

Based on our findings, a simplified schematic is proposed to explain the stability during the carbonation/calcination cycles of CaO supported on KIT-6 (CaK-2), as illustrated in Fig. 8. The major limitation of the commercial CaO, in particular at high temperature, is the low resistance to particle sintering during carbon capture process. However, after the incorporation of CaO into KIT-6, the three-dimensional mesoporous structure of KIT-6 is filled/capped with Ca(NO₃)₂ which through thermal processing with the formation of an interfacial calcium silicate. Further increase of CaO loading results in a complete pore filling/blockage and subsequent agglomeration of CaO, which is the active sites for CO₂ capture, observed by electron microscopy in Figs. 4 and 5. Whilst the formation of the mixed oxide phase results in the reduction of CO₂ uptake, it is beneficial acting as a physical barrier to retard the sintering of the CaO adsorbent particles. Thus, a high stability CaO adsorbent supported by KIT-6 was obtained.

4. Conclusions

In this study, CaO deposited on KIT-6 mesoporous silica has been

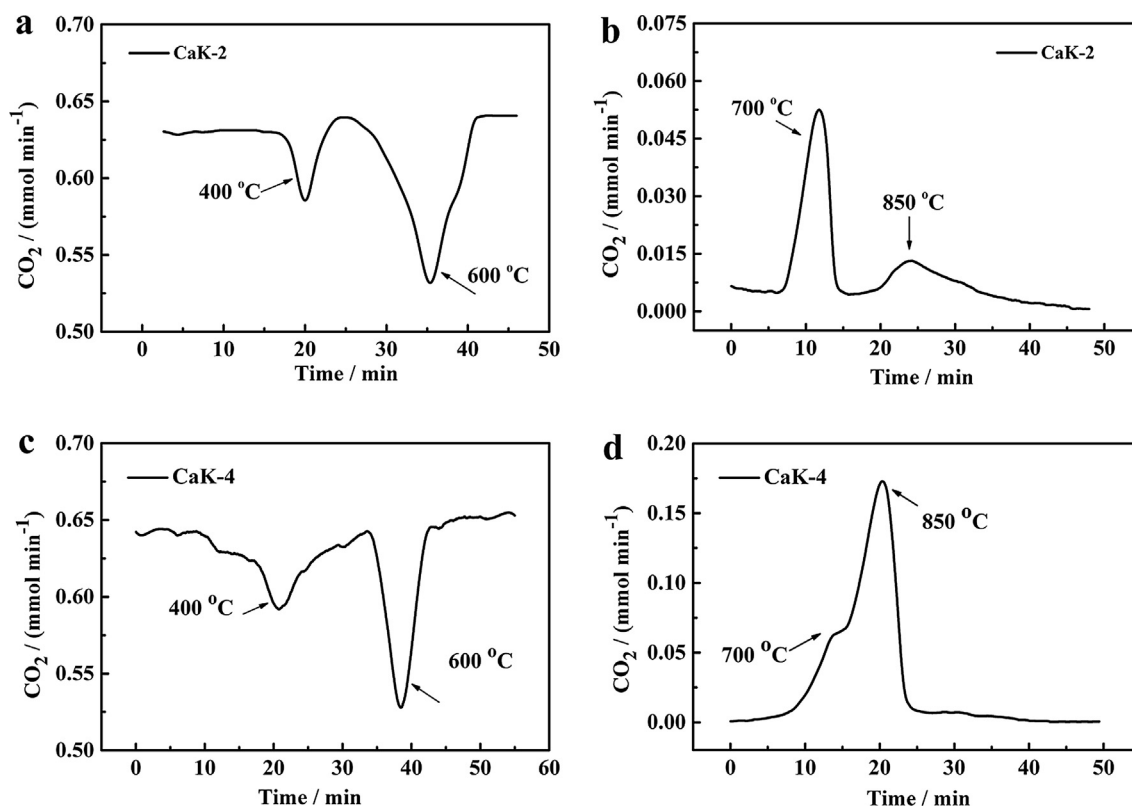


Fig. 7. Fixed bed CO_2 capture performance of different adsorbents (a: carbonation of CaK-2; b: calcination of CaK-2; c: carbonation of CaK-4; d: calcination of CaK-4).

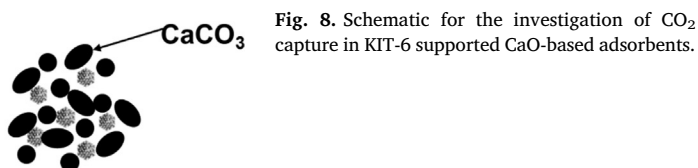
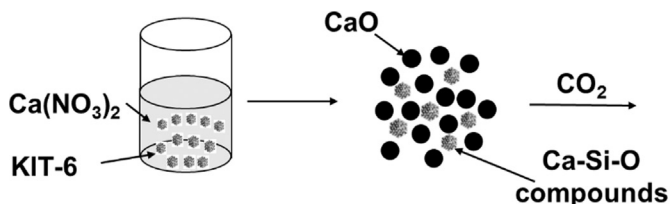


Fig. 8. Schematic for the investigation of CO_2 capture in KIT-6 supported CaO-based adsorbents.

synthesized as adsorbent for high-temperature CO_2 capture. An optimal mass ratio of CaO to KIT-6 was 2:1 (CaK-2) in relation to the stability of adsorbent. The CaK-2 adsorbent possesses a CO_2 capacity of 7.6 mmol g^{-1} . In comparison with a commercial CaO derived from limestone, this new material is able to provide an excellent stability over 10 cycles of carbonation/calcination. This phenomenon is attributed to the three-dimensional structure of KIT-6 and the resulting high degree of interaction between the inert support and active CaO particles, through the formation of mixed oxide interface species, which enhance the sintering-resistant ability of the CaO-based adsorbents.

Acknowledgements

The authors are grateful for the financial support of China Scholarship Council (CSC, no. 201604532), Hebei University of Technology and Open Fund of Key Laboratory of Ocean Energy Utilization and Energy Conservation of Ministry of Education at Dalian University of Technology.

References

- [1] Prathap A, Shaijumon M, Sureshan K. CaO nanocrystals grown over SiO_2 microtubes for efficient CO_2 capture: organogel sets the platform. *Chem Commun* 2016;52:1342–5.
- [2] Ping H, Wu S. CO_2 sorption durability of Zr-modified nano-CaO sorbents with cage-like hollow sphere structure. *ACS Sustain Chem Eng* 2016;4:2047–55.
- [3] Wang Y, Zhang W, Li R, et al. Design of stable cage-like CaO/CaZrO₃ hollow spheres for CO_2 capture. *Energy Fuel* 2016;30:1248–55.
- [4] Yu K, Curcic I, Gabriel J, et al. Recent advances in CO_2 capture and utilization. *ChemSusChem* 2008;1:893–9.
- [5] Hu Y, Liu W, Chen H, et al. Screening of inert solid supports for CaO-based sorbents for high temperature CO_2 capture. *Fuel* 2016;181:199–206.
- [6] Obergassel W, Arens C, Hermwille L, et al. Phoenix from the ashes: an analysis of the Paris Agreement to the United Nations framework convention on climate change. *Wuppertal Institut für Klima, Umwelt, Energie*; 2016.
- [7] Peng W, Xu Z, Zhao H. Batch fluidized bed test of SATS-derived CaO/TiO₂-Al₂O₃ sorbent for calcium looping. *Fuel* 2016;170:226–34.
- [8] Dou B, Song Y, Liu Y, et al. High temperature CO_2 capture using calcium oxide sorbent in a fixed-bed reactor. *J Hazard Mater* 2010;183:759–65.
- [9] Dou B, Zhang H, Cui G, et al. Hydrogen production by sorption-enhanced chemical looping steam reforming of ethanol in an alternating fixed-bed reactor: sorbent to catalyst ratio dependencies. *Energy Convers Manage* 2018;155:243–52.
- [10] Duyar MS, Trevino MAA, Farrauto RJ. Dual function materials for CO_2 capture and conversion using renewable H₂. *Appl Catal B: Environ* 2015;168:370–6.
- [11] Alonso M, Criado Y, Abanades J, et al. Undesired effects in the determination of CO_2 carrying capacities of CaO during TG testing. *Fuel* 2014;127:52–61.
- [12] Perejón A, Romeo LM, Lara Y, et al. The calcium-looping technology for CO_2 capture: on the important roles of energy integration and sorbent behavior. *Appl Energy* 2016;162:787–807.
- [13] Zhao P, Sun J, Li Y, et al. Synthesis of efficient CaO sorbents for CO_2 capture using a simple organometallic calcium-based carbon template route. *Energy Fuel* 2016;30:7543–50.
- [14] Liu W, Low N, Feng B, et al. Calcium precursors for the production of CaO sorbents for multicycle CO_2 capture. *Environ Sci Technol* 2009;44:841–7.
- [15] Manovic V, Anthony E. Steam reactivation of spent CaO-based sorbent for multiple CO_2 capture cycles. *Environ Sci Technol* 2007;41:1420–5.
- [16] Heesink A, Prins W, Van Swaaij W. A grain size distribution model for non-catalytic gas-solid reactions. *Chem Eng J Biochem Eng J* 1993;53:25–37.
- [17] Stendardo S, Foscolo P. Carbon dioxide capture with dolomite: a model for gas-solid reaction within the grains of a particulate sorbent. *Chem Eng Sci* 2009;64:2343–52.

- [18] Wu Y, Blamey J, Anthony E, et al. Morphological changes of limestone sorbent particles during carbonation/calcination looping cycles in a thermogravimetric analyzer (TGA) and reactivation with steam. *Energy Fuel* 2010;24:2768–76.
- [19] Yu F, Phalak N, Sun Z, et al. Activation strategies for calcium-based sorbents for CO₂ capture: a perspective. *Ind Eng Chem Res* 2011;51:2133–42.
- [20] Li Y, Zhao C, Chen H, et al. Modified CaO-based sorbent looping cycle for CO₂ mitigation. *Fuel* 2009;88:697–704.
- [21] Albrecht K, Wagenbach K, Satrio J, et al. Development of a CaO-based CO₂ sorbent with improved cyclic stability. *Ind Eng Chem Res* 2008;47:7841–8.
- [22] Li Z, Cai N, Huang Y, et al. Synthesis, experimental studies, and analysis of a new calcium-based carbon dioxide absorbent. *Energy Fuel* 2005;19:1447–52.
- [23] Zhang X, Li Z, Peng Y, et al. Investigation on a novel CaO-Y₂O₃ sorbent for efficient CO₂ mitigation. *Chem Eng J* 2014;243:297–304.
- [24] Wang S, Fan S, Fan L, et al. Effect of cerium oxide doping on the performance of CaO-based sorbents during calcium looping cycles. *Environ Sci Technol* 2015;49:5021–7.
- [25] Aihara M, Nagai T, Matsushita J, et al. Development of porous solid reactant for thermal-energy storage and temperature upgrade using carbonation/decarbonation reaction. *Appl Energy* 2001;69:225–38.
- [26] Koirala R, Gunugunuri K, Pratsinis S, et al. Effect of zirconia doping on the structure and stability of CaO-based sorbents for CO₂ capture during extended operating cycles. *J Phys Chem B* 2011;115:24804–12.
- [27] Zhao M, Yang X, Church T, et al. Novel CaO-SiO₂ sorbent and bifunctional Ni/Co-CaO/SiO₂ complex for selective H₂ synthesis from cellulose. *Environ Sci Technol* 2012;46:2976–83.
- [28] Kim S, Ida J, Gulians V, et al. Tailoring pore properties of MCM-48 silica for selective adsorption of CO₂. *J Phys Chem B* 2005;109:6287–93.
- [29] Huang C, Chang K, Yu C, et al. Development of high-temperature CO₂ sorbents made of CaO-based mesoporous silica. *Chem Eng J* 2010;161:129–35.
- [30] Wu S, Lan P. A kinetic model of nano-CaO reactions with CO₂ in a sorption complex catalyst. *AIChE J* 2012;58:1570–7.
- [31] Broda M, Kierzkowska AM, Baudouin D, et al. Sorbent-enhanced methane reforming over a Ni-Ca-based, bifunctional catalyst sorbent. *ACS Catal* 2012;2:1635–46.
- [32] Chi C, Li Y, Ma X, et al. CO₂ capture performance of CaO modified with by-product of biodiesel at calcium looping conditions. *Chem Eng J* 2017;326:378–88.
- [33] Haszeldine RS. Carbon capture and storage: how green can black be? *Science* 2009;325:1647–52.
- [34] Hu Y, Liu W, Sun J, et al. High temperature CO₂ capture on novel Yb₂O₃-supported CaO-based sorbents. *Energy Fuel* 2016;30:6606–13.
- [35] Jiang L, Hu S, Syed-Hassan S, et al. Performance and carbonation kinetics of modified CaO-based sorbents derived from different precursors in multiple CO₂ capture cycles. *Energy Fuel* 2016;30:9563–71.
- [36] Kierzkowska A, Pacciani R, Müller C. CaO-based CO₂ sorbents: from fundamentals to the development of new, highly effective materials. *Chemsuschem* 2013;6:1130–48.
- [37] Bhatia S, Perlmutter D. Effect of the product layer on the kinetics of the CO₂-lime reaction. *AIChE J* 1983;29:79–86.